nature COMMUNICATIONS

ARTICLE

Received 13 Dec 2015 | Accepted 1 Dec 2016 | Published 20 Jan 2017

DOI: 10.1038/ncomms14138 OPEN

The shape of telephone cord blisters

Yong Ni[1], Senjiang Yu[2], Hongyuan Jiang[1] & Linghui He[1]

Formation of telephone cord blisters as a result of buckling delamination is widely observed in many compressed film-substrate systems. Here we report a universal morphological feature of such blisters characterized by their sequential sectional profiles exhibiting a butterfly shape using atomic force microscopy. Two kinds of buckle morphologies, light and heavy telephone cord blisters, are observed and differentiated by measurable geometrical parameters. Based on the Föppl-von Kármán plate theory, the observed three-dimensional features of the telephone cord blister are predicted by the proposed approximate analytical model and simulation. The latter further replicates growth and coalescence of the telephone cord into complex buckling delamination patterns observed in the experiment.

[1] CAS Key Laboratory of Mechanical Behavior and Design of Materials, Department of Modern Mechanics, University of Science and Technology of China, Hefei, Anhui 230026, China. [2] Department of Physics, China Jiliang University, Hangzhou 310018, China. Correspondence and requests for materials should be addressed to H.J. (email: jianghy@ustc.edu.cn).

Detailed origins of postbuckling phenomena have been a subject of discussions for several decades[1]. The buckles usually involve multiple instabilities and exhibit intriguing morphologies[2,3]. When a film deposited on a substrate is subject to a large residual compression, it buckles and delaminates away from the substrate, and the blisters with straight-sided, circular, telephone cord (TC) or network-like patterns are formed[4,5]. Predicting the shape of such blisters is of scientific interest for stress-driven pattern formation and important for avoiding structural failure in various film-substrate systems[4]. Among various manifestations of this phenomenon, the TC blister is the most frequently observed in many different film-substrate systems[5]. This motivates a search to identify universal features of TC blisters. Recently, TC formation has been considered as a development from a secondary instability of straight-sided or circular blisters. The instability condition has been analytically addressed by the Föppl-von Kármán (FvK) plate model[6–9]. Further, it has been found that the TC blister can also grow with the appearance of sags by an oscillatory process and its edge unnecessarily starts straight[10,11]. So far, a convincing solution for the three-dimensional (3D) TC blister morphology remains a challenge because of limited methods for handling nonlinear elasticity of thin plate, although a series of numerical models and experiments have provided valuable insights into the morphological features of TC blisters[10–25].

The elegant instability analysis of a straight-sided blister predicted a constant undulation-period-to-width ratio of the TC buckle under the clamping boundary conditions close to the experimental observation[8]. In addition, the ratio may be not constant and change with the interfacial adhesion and the film-to-substrate modulus ratio[11–16]. The zigzag undulation feature of the TC buckle has been replicated by numerical investigations[5,15–19]. A comprehensive study for the 3D TC morphology suggested that it could be approximately viewed as a sequence of connected segments of a circular buckle pinned at its centre[12]. However, such approximation predicted the ridge of the TC blister to be discontinuous, different from our following refined experimental observations wherein the ridge is continuous and its height is periodically changing.

Here we aim to probe the 3D features of the TC morphology using a combination of analytical model, numerical simulation and atomic force microscopy (AFM) study. As shown in Fig. 1a,b, two typical TC blister shapes, light and heavy TC blisters, can be observed in compressed $SiAlN_x$ films on glass substrates. Our experimental observation based on the optical images in Fig. 1a,b indicates that the projected area of the delamination zone of the TC blister is similar to the area swept by a segment of width $2b$ perpendicularly to a sinusoidal centreline. We then assume that the shape of the TC blister can thus be modelled as the postbuckling morphology of the thin plate clamped along such delamination boundary under equal biaxial residual compression (Fig. 1c). An approximate analytical solution for the shape of the TC blister is obtained in the following part. We argue that the shape of the TC blister can be characterized by several sectional profiles perpendicular to the centreline of the delamination zone (Fig. 1c). In contrast to the fact that the sectional profile of the straight-sided blister is always symmetric, the corresponding profile of the TC blister becomes asymmetric, dependent on the wavy amplitude of the centreline. The sequential sectional profiles of the TC blister exhibit a butterfly shape. Such geometric feature becomes more significant in the case of larger waviness amplitude of the centreline, corresponding to a transition from the light TC blister to the heavy TC blister.

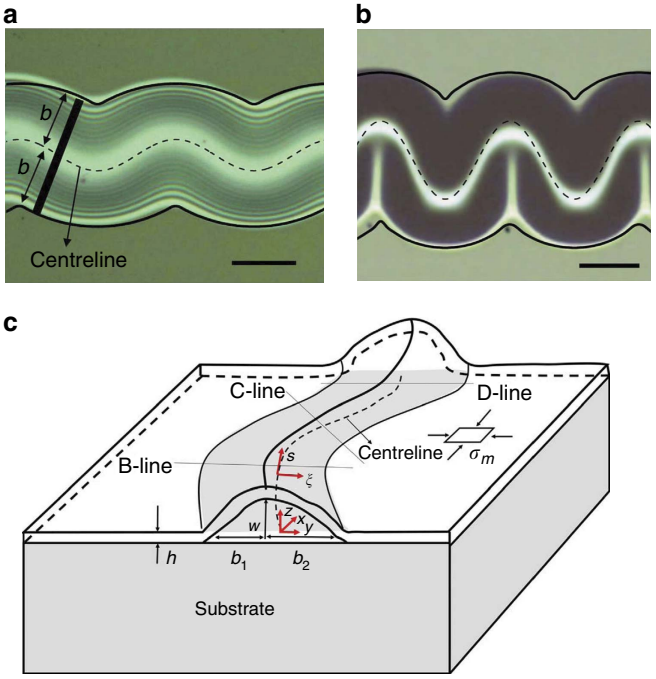

Figure 1 | Schematic model for the shape of telephone cord blisters. Fitting the projected area of (**a**) a light TC blister and (**b**) a heavy TC blister observed in $SiAlN_x$ films on glass substrates. (**c**) Sketch of the FvK model in a curvilinear coordinate under the clamping boundary condition along the boundary of the projected area. Scale bars in (**a**) and (**b**) are 30 and 50 μm, respectively.

Results

Analytical solution to the 3D profile of TC blisters. We firstly determine the 3D shape of the TC blister by solving the FvK equations for a plate of thickness h clamped along the delamination boundary in a curvilinear coordinate (Fig. 1c). The centreline of the delamination zone is described by $\mathbf{r}_0 = [x, A\sin(2\pi x/\lambda), 0]$, where A and λ are the amplitude and the wavelength of the wavy centreline, respectively. The shape of the TC buckles reflected by the profile of the mid-plane of the thin plate after deformation can be expressed as

$$\mathbf{r} = [x - (\xi + u)\sin\theta, A\sin(2\pi x/\lambda) + (\xi + u)\cos\theta, w] \quad (1)$$

where $\theta(x)$ is defined as the angle between the tangential of the centreline and x axis, (s, ξ) is a curvilinear coordinate, $u(s, \xi)$ is the displacement along ξ direction and $w(s, \xi)$ is the deflection of the plate. Here we have assumed that the displacement change along the S direction is negligible compared to $u(s, \xi)$ and $w(s, \xi)$. The edges of the TC buckles are clamped at $\xi = \pm b$. We also assume that the in-plane displacement is small, that is, $u \ll \xi$, $u\frac{\mathrm{d}\theta}{\mathrm{d}s} \ll \frac{\partial u}{\partial \xi}$, and the out-of-plane deflection is relatively large. Based on the observed morphology of the TC buckles, we make another important assumption that u and w change slowly in the S direction, that is, $\frac{\partial u}{\partial s} \ll \frac{\partial u}{\partial \xi}$ and $\frac{\partial w}{\partial s} \ll \frac{\partial w}{\partial \xi}$. We derive the FvK equations with the boundary condition in the curvilinear coordinate by minimizing the total elastic energy in the plate (see the details in the Supplementary Note 1 for the analytical solution to the TC buckle). The strain energy of the TC buckle within a period can be written as

$$\Phi = \int_0^{s_0}\int_{-b}^{b} \phi\sqrt{g}\,\mathrm{d}\,\xi\mathrm{d}s \quad (2)$$

where g is the determinant of the metric tensor $g_{\alpha\beta}$ and therefore $\sqrt{g}\mathrm{d}\xi\mathrm{d}s$ is the element of the area, ϕ is the elastic strain energy

density per unit area having the form

$$\phi = \frac{h}{2} D^{\alpha\beta\rho\mu}\gamma_{\alpha\beta}\gamma_{\rho\mu} + \frac{h^3}{24} D^{\alpha\beta\rho\mu}\Delta\kappa_{\alpha\beta}\Delta\kappa_{\rho\mu} \qquad (3)$$

where $\gamma_{\alpha\beta}$, $\Delta k_{\alpha\beta}$ and $D^{\alpha\beta\rho\mu}$ are defined as the mid-plane Lagrange strain tensor, the curvature change tensor due to deformation and the tensor of the elastic constants in the curvilinear coordinate, respectively. They can be explicitly expressed as a function of the variables s, ξ, u and w. Here the prime denotes differentiation with respect to ξ. If we only keep the leading order term of $u' + \frac{1}{2}(w')^2$, the element of area $\sqrt{g} \approx 1 - \xi\theta_{,s}$ with $\theta_{,s} = \frac{-Aq^2\sin(qx)}{[1+A^2q^2\cos^2(qx)]^{3/2}}$. The arc length of the centreline $s(x)$ is given by $\mathrm{d}s = \sqrt{1+A^2q^2\cos^2(qx)}\mathrm{d}x$, with $q = 2\pi/\lambda$. We also assume that $s = 0$ at $x = 0$ and $s = s_0$ at $x = 2\pi/q$. From $\delta\Phi/\delta u = 0$, we have the in-plane equilibrium equation of the plate

$$t_a' = 0 \qquad (4)$$

where $t_a = \bar{E}_f h\sqrt{g}\left[(1+v)\varepsilon_m + u' + \frac{1}{2}(w')^2\right]$ is the membrane stress along the direction of ξ in the film. $\bar{E}_f = \frac{E}{1-v^2}$ is plane strain modulus with E, v the Young's modulus and the Poisson's ratio of the plate, respectively. ε_m is the uniform equibiaxial residual strain in the plate. Equation (4) indicates the membrane stress t_a should be a constant. Similarly, from $\delta\Phi/\delta w = 0$ we obtain the out-of-plane equilibrium equation of the plate

$$\left[(1-\xi\theta_{,s})w''\right]'' - \left[\lambda w' + \frac{\theta_{,s}^2}{1-\xi\theta_{,s}}w'\right]' = 0 \qquad (5)$$

where $\lambda = \frac{12t_a}{\bar{E}_f h^3}$. By solving equations (4) and (5) as an eigenvalue problem, we get an approximate solution to the deflection of the plate up to the first order

$$w(x,\xi) \approx w_0\left\{\frac{1}{2}\left(1-\frac{1}{4}\theta_{,s}\xi\right)\left[1+\cos\left(\frac{\pi}{b}\xi\right)\right] + \frac{\pi}{4b}\theta_{,s}(b^2-\xi^2)\sin\left(\frac{\pi}{b}\xi\right)\right\} \qquad (6)$$

where w_0 is an unknown constant. Equation (6) is reduced to $w(x,\xi) = \frac{1}{2}w_0\left[1+\cos\left(\frac{\pi}{b}\xi\right)\right]$ for the buckling of a straight strip with uniform width ($\theta_{,s} = 0$) (ref. 6). Therefore, w_0 represents the maximum deflection of the plate when $\theta_{,s} = 0$. Note that $t_a = -\frac{\bar{E}_f h^3}{12}\left(\frac{\pi}{b}\right)^2$ at $\theta_{,s} = 0$. Integrate this equation from $-b$ to b, and notice that $u = 0$ at $\xi = \pm b$, one can get

$$w_0^2 = -\frac{640[12b^2\varepsilon_m(1+v) + h^2\pi^2]}{480\pi^2 + (-465 - 110\pi^2 + 16\pi^4)b^2\theta_{,s}^2} \qquad (7)$$

The characteristic shape of TC blisters. Equation (6) together with equation (7) provides for the first time an approximate analytical solution to the 3D profile of the TC buckle after the specific delamination area is available. To test whether the solution can predict the 3D feature of the TC blister shape or not, Fig. 2 plots several sectional profiles of a buckled tantalum (Ta) film on glass substrates perpendicular to the centreline shown in the inserted modified AFM image with the size of 40 μm × 40 μm. The result in Fig. 2 shows that the sequence of the sectional profiles of the TC blister perpendicular to the centreline exhibits a butterfly shape reminiscent of the butterfly curve of strain versus applied load in shape memory alloys. The asymmetry is characterized by two different half-separations denoted by b_1 and b_2 based on the ridge line of the TC blister (see Fig. 1c). The asymmetry has a maximum in the profile along B-line or D-line, while the profile along the C-line is symmetric. In addition, the maximum deflection in each sectional profile corresponding to the point at the ridge line is not constant. It has the smallest value in the profile along the C-line and the largest value in the profile along the B-line or D-line. This geometric feature of the TC blister is different from the previous report[12] wherein the ridge line is viewed as a discontinuous contour line. Figure 2 demonstrates that the theoretical result obtained by equation (6) predicts the asymmetric 3D feature of the TC blister, and the deflection amplitude variation of the TC ridge line. This is consistent with the AFM measurements after the measured parameters of the buckled Ta film is given as $h = 225$ nm, $b = 10$ μm, $\lambda/b = 2$, $A/\lambda = 0.08$, and the residual strain in the Ta film is assumed to be $\varepsilon_m = 0.004$. The deflection amplitude of the ridge line given by equation (6) is underestimated because of the assumption of rigid substrate and clamping boundary condition. In fact, the substrate compliance could increase the maximum deflection[26]. We further numerically track the postbuckling morphology of the compressed plate on the substrate by setting the same predelamination zone, the same residual stress and the same other material parameters as those in the case of the analytical solution. The film-to-substrate modulus ratio is set to be 2.5 (about 70 GPa for the glass substrate and 175 GPa for Ta film) based on the continuum model[15]. The numerical result in Fig. 2 matches the experimentally observed morphological feature of the TC blister even more closely.

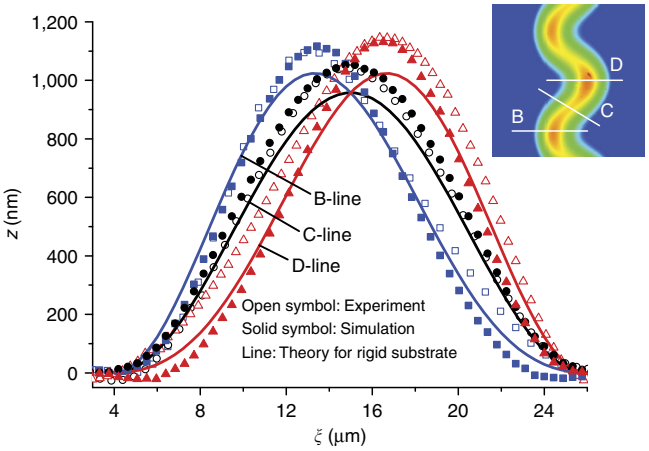

Figure 2 | Characterization of the TC blister shape. Several sectional profiles perpendicular to the centreline are shown in the inserted modified AFM image 40 μm × 40 μm, which is updated by manually performing planefit offline of the original AFM image obtained by line-by-line (256 lines) scanning modes. The results from theory, simulation and AFM measurements are compared in a Ta film on glass substrates.

The approximate solution in equation (6) also predicts the asymmetry denoted by b_1/b_2 and the variation of the maximum deflection at the ridge of the TC blister denoted by $w^{\max}_{\text{C-line}}/w^{\max}_{\text{B-line}}$ as a function of the waviness of the centreline denoted by A/λ. In the limit of $A/\lambda = 0$, $b_1/b_2 = 1$ and $w^{\max}_{\text{C-line}}/w^{\max}_{\text{B-line}} = 1$, it is the case of a straight-sided blister. The stability analysis for the straight-sided blister only predicted the onset stage during formation of the TC blister, namely, the amplitude of the undulation is infinitely small corresponding to $A/\lambda \to 0$ (ref. 8). The current solution can apply to the case with finite value of A/λ. Figure 3 shows that different undulatory shapes of the TC blisters can be described by two measurable geometrical parameters b_1/b_2 and $w^{\max}_{\text{C-line}}/w^{\max}_{\text{B-line}}$ as a function of A/λ with the comparison between theory, simulation and experimental observations in various films including Ta, $SiAlN_x$, Fe and Ni on glass substrates. With the increase of A/λ, the values of b_1/b_2 and $w^{\max}_{\text{C-line}}/w^{\max}_{\text{B-line}}$ more significantly deviate from one, corresponding to the larger asymmetry. However, we must note that the approximate analytical solution is reliable only when the value of A/λ is very

small since it proceeds by an asymptotic expansion in $\theta_{,s}$ (see the details in the Supplementary Note 1 for analytical solution to the TC buckle). From equation (5) it indicates that the solution may be questionable since there is a singularity as $1-\xi\theta_{,s}=0$. The singularity disappears when $A/\lambda<1/(2\pi^2)=0.05$ at $\lambda=2b$. For the larger value of A/λ, the numerical solution[15] is more close to the experimental data, as shown in Fig. 3. It is found that the variations of b_1/b_2 and $w^{\max}_{\mathrm{C-line}}/w^{\max}_{\mathrm{B-line}}$ tend to be saturated, respectively, after $A/\lambda>0.08$, in contrast to the monotonous deviation from one predicted by the approximate analytical solution. The result in Fig. 3 thus demonstrates that b_1/b_2 and $w^{\max}_{\mathrm{C-line}}/w^{\max}_{\mathrm{B-line}}$ are another two measurable geometric parameters to characterize the undulatory morphology of the TC blister beside of λ/b and A/λ. The dependence of b_1/b_2 and $w^{\max}_{\mathrm{C-line}}/w^{\max}_{\mathrm{B-line}}$ on A/λ is attributed to the fact that the wavy centreline of the delamination zone breaks the symmetry with respect to the straight centreline and introduces a position-dependent curvature as indicated in Supplementary Equation (10) in the buckled film wherein the buckling across the centreline may be not symmetric anymore.

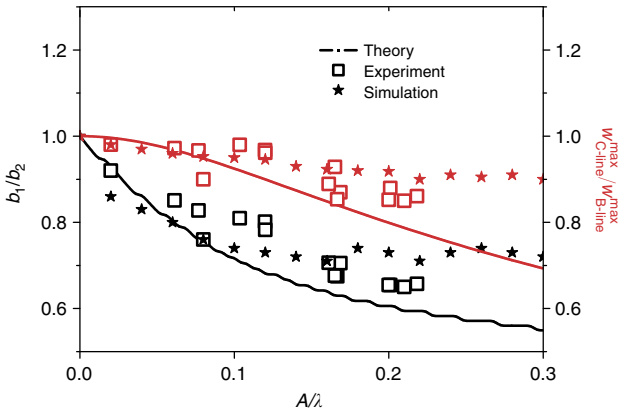

Figure 3 | Measurable geometrical parameters. b_1/b_2 and $w^{\max}_{\mathrm{C-line}}/w^{\max}_{\mathrm{B-line}}$ as a function of A/λ characterize different undulatory shapes of the TC blisters: comparison between theory, simulation and experimental observations in various films including Ta, $SiAlN_x$, Fe and Ni on glass substrates.

Light and heavy TC blisters. Figure 4 demonstrates that there are two kinds of buckle morphologies, light and heavy TC blisters, differentiated by the value of A/λ. The upper row in Fig. 4 is the experimental observation in Ta and $SiAlN_x$ films on glass substrates, respectively. The lower row in Fig. 4 is the simulated postbuckling morphology given $b/h=49$, $\lambda/b=2$ and $\varepsilon_m=0.005$ at different values of A/λ. It is found that with the increase of A/λ, the buckle really turns out to be ubiquitously undulated from light to heavy TC blisters. The obtained result is consistent with the experimental observation shown in Supplementary Movie 1, where an initially straight blister progressively grows into the familiar TC structure. We believe that the transition point between the light and heavy TC blisters depends on the value of A/λ. In the light TC blister, the value of A/λ is very small, the width of the delamination area is close to $2b$, the delamination boundary is smooth and the values of b_1/b_2 and $w^{\max}_{\mathrm{C-line}}/w^{\max}_{\mathrm{B-line}}$ monotonously deviate from one. In contrast, in the heavy TC blister, the value of A/λ is much larger, the delamination zone significantly widens, the values of b_1/b_2 and $w^{\max}_{\mathrm{C-line}}/w^{\max}_{\mathrm{B-line}}$ are saturated, and the delamination boundary shows a cusp indicating the existence of a singularity (see Supplementary Fig. 3).

In our analytical approach, λ/b and A/λ extracted from the projected area of the TC blister are assumed to be the input parameters instead of the prediction. Based on the assumption, the equilibrium values of b_1/b_2 and $w^{\max}_{\mathrm{C-line}}/w^{\max}_{\mathrm{B-line}}$ that quantify the typical 3D features of the TC blister are determined by the postbuckling solution given delamination area. We can obtain the values of λ/b and A/λ from the experimental observation. The measurement of λ/b is straightforward[12]. While the measurement of A/λ could be obtained by tracking the undulation of the ridge line denoted by A'/λ, which value could be roughly viewed as that of A/λ (Fig. 1a,b). The results

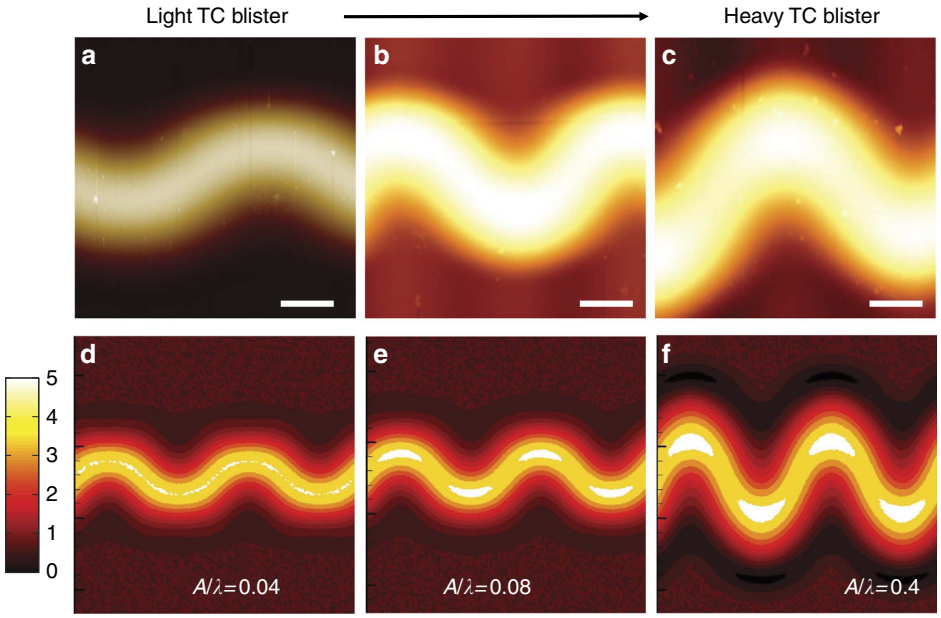

Figure 4 | Morphologies of light and heavy TC blisters. (**a**–**c**) AFM images. Scale bars are 10 μm. (**d**–**f**) Numerical simulation results with parameters $b/h=49$, $\lambda/b=2$, $\varepsilon_m=0.005$, and $A/\lambda=0.04$, 0.08 and 0.4.

shown in Supplementary Fig. 2 indicate that both values of λ/b and A'/λ in various observed TC blisters tend to be saturated and fall into a narrow range. The value of the former is between 1.6 and 2.8, consistent with the report in the literature[16]. The value of the latter is between 0.1 and 0.3. Since the TC blister can be developed from a secondary buckling instability of a straight-sided blister, where the instability mode predicts $\lambda/b \approx 2$ given the parameters b and $A = 0$ (ref. 8), we believe that the waviness period of the TC blister may be inherited from the instability wavelength. The deviation from $\lambda/b \approx 2$ is attributed that λ/b also depends on the adhesion with a non-trivial relationship[14,16]. Usually the increase of A/λ releases more the elastic energy in the biaxially compressed film deposited on the substrate, while it has to increase the mixed-mode-dependent adhesion energy. The competition between them sets the equilibrium value of A/λ. In addition, large value of A/λ in the TC blisters is hard to report. It is possible because the case with a large value of A/λ definitely increases the stress concentration which may lead to ridge crack[20] or further buckling bifurcation, and the buckle is not TC blister any more[15].

Up to now, our modelling to the shape of the TC blister is obtained under the particular assumption on the shape of the delamination region. In fact, the delamination area is unnecessary to be sinusoidal shaped, especially during the oscillatory growth process of the TC blister[11]. Usually, determination of the buckle–delamination morphology can be separated into two steps. The first step is to derive a postbuckling solution given the delamination zone. The second step is to determine the delamination zone at equilibrium. If the edge of the delamination zone is described as the interfacial crack front, the delamination zone at equilibrium is determined as the buckling-mediated energy release rate is equal to the interface toughness. For the straight-sided blister, both steps are done analytically[6]. However, the analytical solution to the second step for the TC blister is not available.

In fact, both the equilibrium delamination area and postbuckling morphology in thin films deposited on substrates can also be theoretically determined in principle. If we further take into account the contribution of the adhesion energy and the elastic strain energy in the substrate, all the equilibrium values of λ/b, A/λ, b_1/b_2 and $w^{\max}_{\mathrm{C-line}}/w^{\max}_{\mathrm{B-line}}$ that quantify the TC blister shape with less restriction can be numerically determined by minimizing the total free energy in the film-substrate system. Our current numerical simulations rely on the recently developed continuum modelling to track the general morphological evolution of the buckle delamination without any restriction of the delamination zone[15]. In this approach, the concurrent buckling and delaminating processes are formulated using the time-dependent Ginzburg–Landau kinetic equations, driven by minimizing the film-substrate total free energy, including the elastic energies in both the film and the substrate, and the mixed-mode interfacial adhesion between them[11,15]. The effect of substrate elasticity and interfacial adhesion on the shape of the TC blister can be taken into account, which is neglected in the analytical approach. The modelling and simulation approach is outlined in Supplementary Note 3 and some results are shown in Supplementary Figs 4–6. The coupling behaviour between buckling and delamination in a film deposited on substrates with higher compressive stresses becomes more complex[20,22], and the TC blister may exhibit beyond the sinusoidal configuration. Our numerical simulations not only recover the growth process of the TC blister from an initially circular blister[7] but also capture a rich coalescence behaviour accompanied with the increase of the buckling width during further propagation of the TC buckle. The TC buckle becomes larger and larger with the appearance of several spikes and/or daughter TC buckle at the outer undulated edge, consistent with our experimental observation (see Supplementary Fig. 6 and Supplementary Movies 2 and 3).

Discussion

In summary, the refined 3D morphological features of the TC buckle are elucidated by using AFM characterization, approximate analytical model and numerical simulations. We confirm that the shape of the TC blister can be modelled as the postbuckling morphology of the compressed plate clamped along the delamination front given the parameters λ/b and A/λ. Two measurable geometrical parameters b_1/b_2 and $w^{\max}_{\mathrm{C-line}}/w^{\max}_{\mathrm{B-line}}$ are proposed to characterize a so-called 'butterfly shape' of the sequential sectional profiles, which are universal in both the light and heavy TC blisters. The above features are successfully reproduced by our approximate analytical model and numerical simulations. Furthermore, how the fully nonlinear buckle-driven delamination process leads to the morphological evolution of the TC blister is captured by numerical simulations and experimental observation. The present work provides insight into the 3D shape of TC buckles.

Methods

Formation of the TC buckle as a result of the buckle-driven delamination process was simulated using the phase field method where the film buckles into an equilibrium buckle–delamination configuration driven by minimizing the total free energy. The total free energy of the film-substrate system is established by incorporating Green function method for the substrate elasticity, FvK plate theory for nonlinear film deformation and cohesive zone model for mixed-mode interfacial adhesion. The total free energy of the film-substrate system including the film, the substrate and the interface can be expressed as a functional of the out-of-plane displacement of the film $\zeta(\mathbf{x}, t)$ and the displacement jump vector across the interface $\Lambda(\mathbf{x}, t)$ as $U^{\mathrm{tot}} = U^{\mathrm{film}} + U^{\mathrm{sub}} + U^{\mathrm{int}}$, where U^{film} is the elastic strain energy including the bending and stretching energies in the film, U^{sub} is the elastic energy of the substrate and U^{int} is the adhesion energy between the film and the substrate. Their detailed expressions are found in ref. 15. Following ref. 11, we may also adopt alternative cohesive zone model with bilinear traction versus separation law for better description of mixed-mode dependence of interface adhesion. The dynamic equations for ζ, Λ_i denoted as the time-dependent Ginzburg–Landau kinetic equations to describe the minimization process of the total free energy are given by: $\partial\zeta/\partial t = -\Gamma_\zeta \delta U^{\mathrm{tot}}/\delta\zeta$ and $\partial\Lambda_i/\partial t = -\Gamma_{\Lambda_i}\delta U^{\mathrm{tot}}/\delta\Lambda_i$, where t denotes time and Γ_ζ, Γ_{Λ_i} are the kinetic coefficients that characterize the relaxation rates of the buckling and delamination processes in the overdamped dynamics. This gradient flow form of the dynamics guarantees a monotonous minimization process of U^{tot} and ensures a convergent solution of the dynamic equations, whose steady-state solutions provide the configuration at the equilibrium. We solve the reduced forms in a computational cell with periodic boundary conditions using input parameters: $\varepsilon^0_{\alpha\beta}$, μ_f/μ_s, $\nu_f = 0.3$, $\nu_s = 0.5$, $\Gamma^*_{\Lambda_i} = \Gamma^*_{\Lambda_i}/\Gamma_\zeta = 0.1$, $\delta_n = \delta_t = 0.2h$, $\gamma^*_n = \gamma_n/e\delta_n\mu_s$ and $\gamma^*_t = \gamma_t/e\delta_n\mu_s$. The grid spacing is $\Delta x = \Delta y = h$ and the time step is $\Delta t = 0.1t/\tau$, with $\tau = h/\Gamma_\zeta\mu_s$. A small random fluctuation mimicking the thermal fluctuation is used to facilitate nucleation of buckling delamination from the pre-existing interfacial delamination region, in which zero interface toughness is assumed.

Data availability. The data that support the findings of this study are available from the corresponding author on request.

References

1. Hutchinson, J. W. & Koiter, W. T. Postbuckling theory. *App. Mech. Rev.* **23,** 1353–1366 (1970).
2. Pocivavsek, L. *et al.* Stress and fold localization in thin elastic membranes. *Science* **320,** 912–916 (2008).
3. Brau, F. *et al.* Multiple-length-scale elastic instability mimics parametric resonance of nonlinear oscillators. *Nat. Phys.* **7,** 56–60 (2011).
4. Freund, L. B. & Suresh, S *Thin Film Materials: Stress, Defect Formation and Surface Evolution* (Cambridge University Press, 2003).
5. Gioia, G. & Ortiz, M. Delamination of compressed thin films. *Adv. Appl. Mech.* **33,** 119–192 (1997).
6. Hutchinson, J. W. & Suo, Z. Mixed-mode cracking in layered materials. *Adv. Appl. Mech.* **29,** 63–191 (1992).

7. Hutchinson, J. W., Thouless, M. D. & Liniger, E. G. Growth and configurational stability of circular, buckling-driven dilm delaminations. *Acta Metall. Mater.* **40,** 295–308 (1992).
8. Audoly, B. Stability of straight delamination blisters. *Phys. Rev. Lett.* **83,** 4124–4127 (1999).
9. Parry, G., Cimetiere, A., Coupeau, C., Colin, J. & Grilhe, J. Stability diagram of unilateral buckling patterns of strip-delaminated films. *Phys. Rev. E* **74,** 066601 (2006).
10. Thouless, M. D. Combined buckling and cracking of films. *J. Am. Ceram. Soc.* **76,** 2936–2938 (1993).
11. Faou, J. Y., Parry, G., Grachev, S. & Barthel, E. How does adhesion induce the formation of telephone cord buckles? *Phys. Rev. Lett.* **108,** 116102 (2012).
12. Moon, M. W., Jensen, H. M., Hutchinson, J. W., Oh, K. H. & Evans, A. G. The characterization of telephone cord buckling of compressed thin films on substrates. *J. Mech. Phys. Solids* **50,** 2355–2377 (2002).
13. Moon, M. W., Lee, K. R., Oh, K. H. & Hutchinson, J. W. Buckle delamination on patterned substrates. *Acta Mater.* **52,** 3151–3159 (2004).
14. Pan, K., Ni, Y. & He, L. H. Effects of interface sliding on the formation of telephone cord buckles. *Phys. Rev. E* **88,** 062405 (2013).
15. Ni, Y. & Soh, A. K. On the growth of buckle-delamination pattern in compressed anisotropic thin films. *Acta Mater.* **69,** 37–46 (2014).
16. Faou, J. Y., Parry, G., Grachev, S. & Barthel, E. Telephone cord buckles—a relation between wavelength and adhesion. *J. Mech. Phys. Solids* **75,** 93–103 (2015).
17. Crosby, K. M. & Bradley, R. M. Pattern formation during delamination and buckling of thin films. *Phys. Rev. E* **59,** R2542 (1999).
18. Peyla, P. Undulated blistering during thin film delamination. *Phys. Rev. E* **62,** R1501 (2000).
19. Jagla, E. A. Modeling the buckling and delamination of thin films. *Phys. Rev. B* **75,** 085405 (2007).
20. Yu, S. J. *et al.* Morphological selections and dynamical evolutions of buckling patterns in $SiAlN_x$ films: from straight-sided to telephone cord or bubble structures. *Acta Mater.* **64,** 41–53 (2014).
21. Liu, Y. P. *et al.* Large-area, periodic, hexagonal wrinkles on nanocrystalline graphitic film. *Adv. Funct. Mater.* **25,** 5492–5503 (2015).
22. Yu, S. J. *et al.* Spatial and kinetic evolutions of telephone cord buckles. *Surf. Coat. Technol.* **228,** 258–265 (2013).
23. Jin, W. M. & Sternberga, P. Energy estimates for the von Kármán model of thin-film blistering. *J. Math. Phys.* **42,** 192–199 (2001).
24. Angelillo, M., Babilio, E., Cardamone, L., Fortunato, A. & Lippiello, M. Some remarks on the retrofitting of masonry structures with composite materials. *Compos Part B* **61,** 11–16 (2014).
25. Belgacem, H. B., Conti, S., DeSimone, A. & Müller, S. Energy scaling of compressed elastic films—three-dimensional elasticity and reduced theories. *Arch. Ration. Mech. Anal.* **164,** 1–37 (2002).
26. Parry, G. *et al.* Effect of substrate compliance on the global unilateral post-buckling of coatings: AFM observations and finite element calculations. *Acta Mater.* **53,** 441–447 (2005).

Acknowledgements

This work was supported by the National Natural Science Foundation of China (Grant Nos 11222219, 11472262, 11132009, 11472271, 11622222 and 11204283), the Collaborative Innovation Center of Suzhou Nano Science and Technology, the Fundamental Research Funds for the Central Universities (Grant Nos WK2090050027 and WK2480000001) and the Strategic Priority Research Program of the Chinese Academy of Sciences (Grant No. XDB22040502 and XDB22040403).

Author contributions

Y. Ni, S. Yu, H. Jiang and L. He initiated and supervised the project. H. Jiang conceived the theory. Y. Ni performed phase field simulation. S. Yu performed AFM measurement. All authors analysed the data and wrote the manuscript.

Additional information

Supplementary Information accompanies this paper at http://www.nature.com/naturecommunications

Competing financial interests: The authors declare no competing financial interests.

Reprints and permission information is available online at http://npg.nature.com/reprintsandpermissions/

How to cite this article: Ni, Y. *et al.* The shape of telephone cord blisters. *Nat. Commun.* **8,** 14138 doi: 10.1038/ncomms14138 (2017).

Publisher's note: Springer Nature remains neutral with regard to jurisdictional claims in published maps and institutional affiliations.

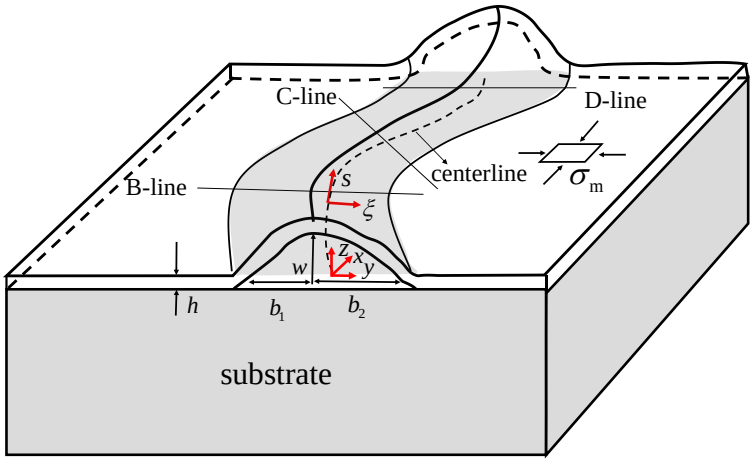

Supplementary Figure 1. sketch of the FvK model in a curvilinear coordinate under the clamping boundary condition along the boundary of the projected area.

(a)

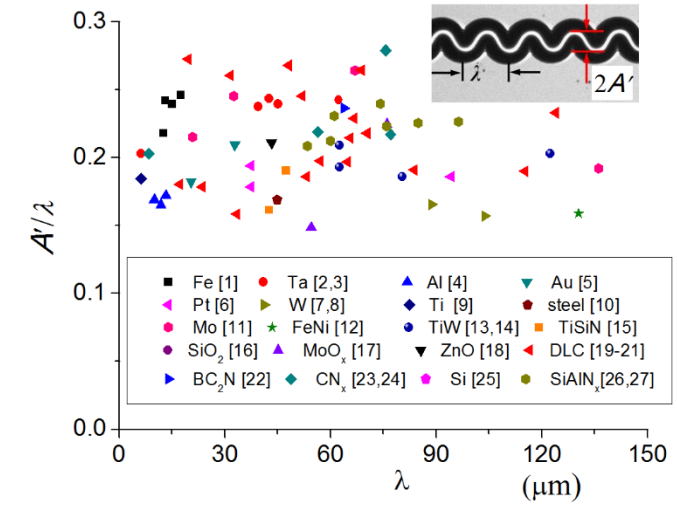

(b)

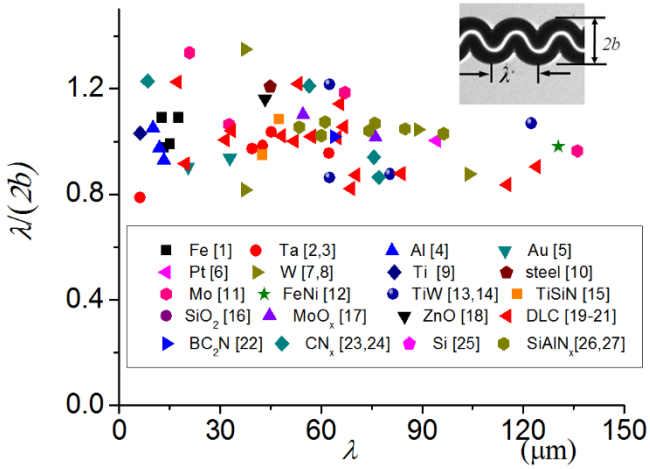

Supplementary Figure 2. Plot of A'/λ and $\lambda/(2b)$ as a function of λ in various TC blister buckles

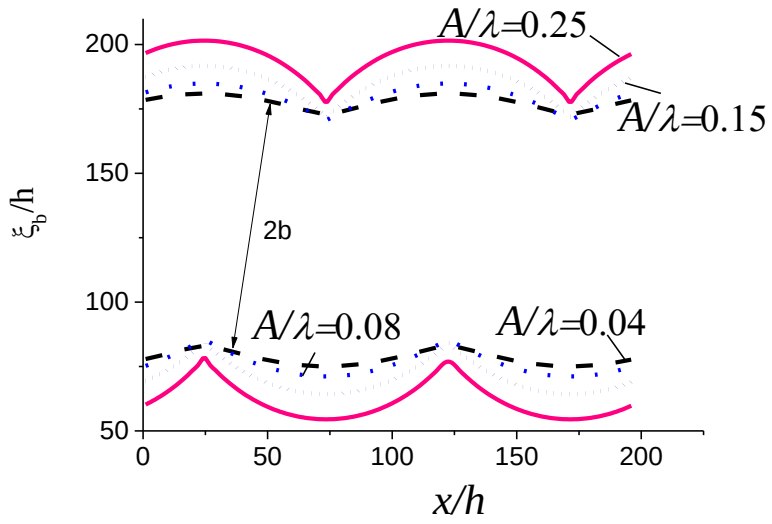

Supplementary Figure 3. Plot of the side undulation curve under different values of A/λ

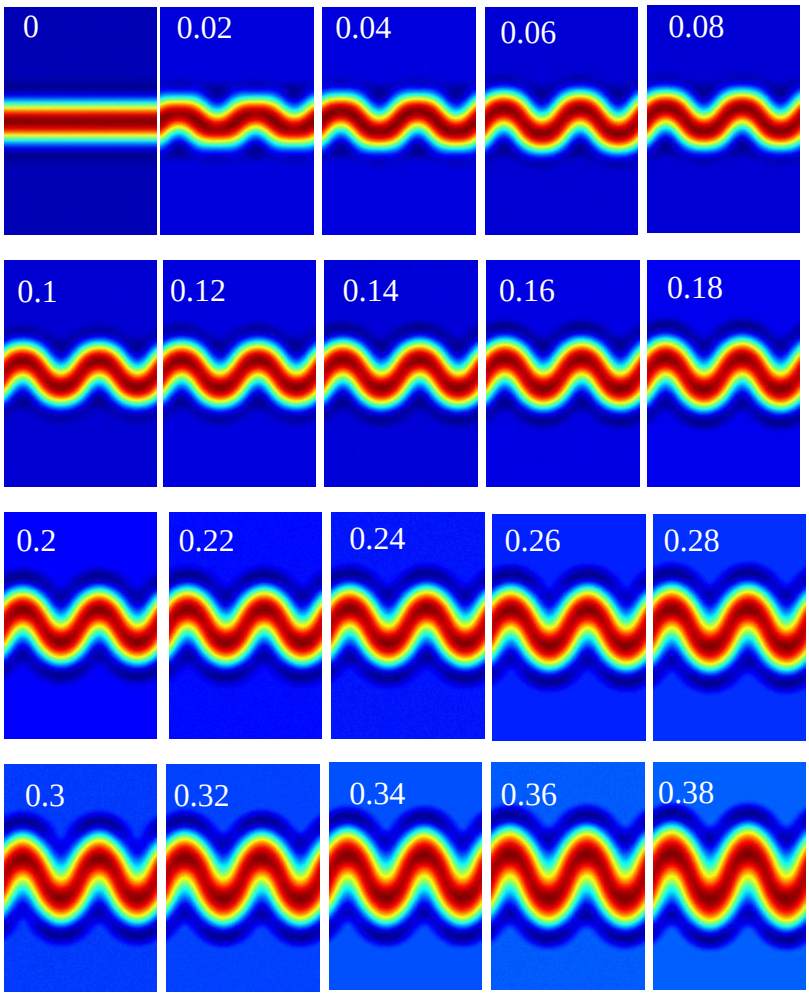

Supplementary Figure 4. The simulated contour map of the post-buckling morphology under different value of A/λ from 0 to 0.38 with the increase of 0.02

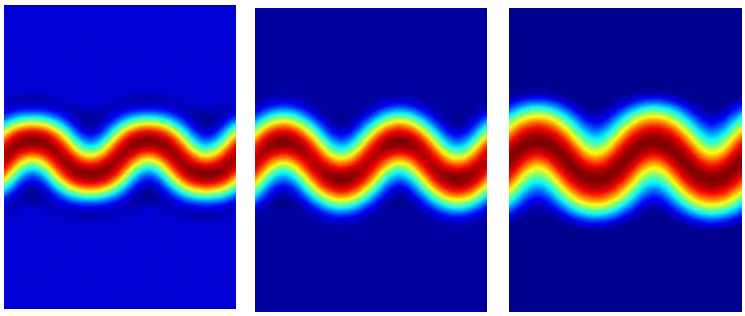

Supplementary Figure 5. Effect of the modulus ratio between film and substrate on the shape of TC blister

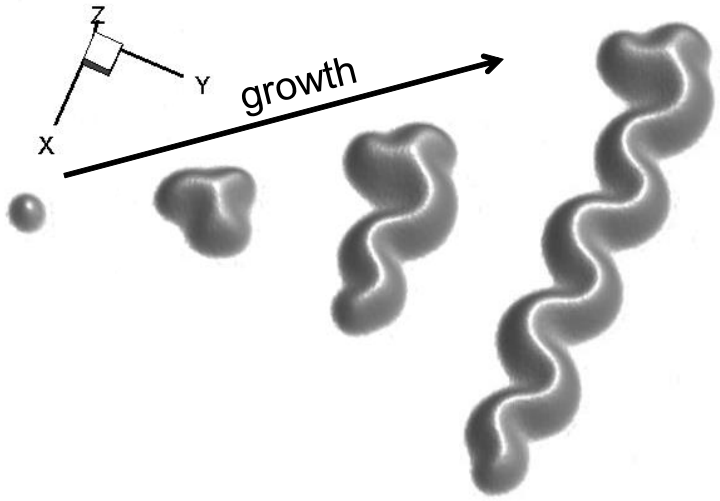

Supplementary Figure 6. The growth of a TC blister obtained by numerical simulation

Supplementary Note 1: Analytical solution to the telephone cord buckle

As shown Supplementary Figure 1, the centerline of the telephone cord can be given by $\mathbf{r}_0 = \left[x, A\sin\left(2\pi x/\lambda\right), 0\right]$ where A and λ are the amplitude and wavelength of the centerline, respectively. The tangent vector of the centerline is $\frac{d\mathbf{r}_0}{dx} = \left[1, -Aq\cos\left(qx\right), 0\right]$ with $q = 2\pi/\lambda$. Therefore, the distance between the two nearby points is

$$ds^2 = \frac{d\mathbf{r}_0}{dx}\cdot\frac{d\mathbf{r}_0}{dx} = \left[1 + A^2q^2\cos^2\left(qx\right)\right]dx^2 \tag{S.1}$$

Define the angle $\theta(x)$ between the tangential of the centerline and x axis so that

$$\begin{aligned}\cos\theta &= \frac{dx}{ds} = \frac{1}{\sqrt{1 + A^2q^2\cos^2\left(qx\right)}}\\ \sin\theta &= \frac{dy}{ds} = \frac{Aq\cos\left(qx\right)}{\sqrt{1 + A^2q^2\cos^2\left(qx\right)}}\end{aligned} \tag{S.2}$$

Therefore, the shape of the telephone cord buckles can be described as

$$\mathbf{r} = \left[x - \left(\xi + u\right)\sin\theta, A\sin\left(qx\right) + \left(\xi + u\right)\cos\theta, w\right] \tag{S.3}$$

where $\left(s, \xi\right)$ is a curvilinear coordinate and $u\left(s, \xi\right)$ is the displacement along ξ direction and $w\left(s, \xi\right)$ is the deflection of the plate. Here, we have assumed that the displacement along the s direction is negligible compared to $u\left(s, \xi\right)$ and $w\left(s, \xi\right)$. The edge of the telephone cord buckles are clamped at $\xi = \pm b$. By considering Eq. (S.2), the local tangential vectors can be written as

$$\begin{aligned}\mathbf{m}_1 &= \frac{\partial\mathbf{r}}{\partial s} = \left[\left[1 - \left(\xi + u\right)\frac{d\theta}{ds}\right]\cos\theta - \frac{\partial u}{\partial s}\sin\theta, \left[1 - \left(\xi + u\right)\frac{d\theta}{ds}\right]\sin\theta + \frac{\partial u}{\partial s}\cos\theta, \frac{\partial w}{\partial s}\right]\\ \mathbf{m}_2 &= \frac{\partial\mathbf{r}}{\partial \xi} = \left[-\left(1 + \frac{\partial u}{\partial \xi}\right)\sin\theta, \left(1 + \frac{\partial u}{\partial \xi}\right)\cos\theta, \frac{\partial w}{\partial \xi}\right]\end{aligned} \tag{S.4}$$

In this work, we assume the in-plane displacement is small, i.e., $u \ll \xi$ and

$u\dfrac{d\theta}{ds} \ll \dfrac{\partial u}{\partial \xi}$, and the out-of-plane deflection is relatively large. From the morphology of telephone cord buckles, we make another important assumption that u and w change slowly in the s direction, i.e., $\dfrac{\partial u}{\partial s} \ll \dfrac{\partial u}{\partial \xi}$ and $\dfrac{\partial w}{\partial s} \ll \dfrac{\partial w}{\partial \xi}$. Therefore, the two tangential vectors can be simplified to

$$\begin{aligned} \mathbf{m}_1 &= \left[\left(1-\xi\theta_{,s}\right)\cos\theta, \left(1-\xi\theta_{,s}\right)\sin\theta, 0\right] \\ \mathbf{m}_2 &= \left[-\left(1+u'\right)\sin\theta, \left(1+u'\right)\cos\theta, w'\right] \end{aligned} \tag{S.5}$$

where $\theta_{,s} \equiv \dfrac{d\theta}{ds}$, $u' \equiv \dfrac{\partial u}{\partial \xi}$ and $w' \equiv \dfrac{\partial w}{\partial \xi}$. Here the prime denotes differentiation with respect to ξ. The metric tensor in the deformed film is given by

$$g_{\alpha\beta} = \mathbf{m}_\alpha \cdot \mathbf{m}_\beta = \begin{bmatrix} \left(1-\xi\theta_{,s}\right)^2 & 0 \\ 0 & \left(1+u'\right)^2 + \left(w'\right)^2 \end{bmatrix} \tag{S.6}$$

Similarly, we can calculate the tangential vectors and therefore obtain the metric tensor in the undeformed film as

$$\bar{g}_{\alpha\beta} = \begin{bmatrix} \left(1-\xi\theta_{,s}\right)^2 & 0 \\ 0 & 1 \end{bmatrix} \tag{S.7}$$

The mid-plane Lagrange strain tensor defined as

$$\gamma_{\alpha\beta} = \frac{1}{2}\left(g_{\alpha\beta} - \bar{g}_{\alpha\beta}\right) + \varepsilon_m \bar{g}_{\alpha\beta} = \begin{bmatrix} \varepsilon_m\left(1-\xi\theta_{,s}\right)^2 & 0 \\ 0 & \varepsilon_m + u' + \dfrac{1}{2}\left(w'\right)^2 \end{bmatrix} \tag{S.8}$$

where ε_m is the uniform equi-biaxial mismatch stress. Here we have used the assumption that $u' \ll 1$. The corresponding mixed component of the mid-plane Lagrange strain tensor is

$$\gamma_\alpha^\beta = \gamma_{\alpha\rho}\bar{g}^{\rho\beta} = \begin{bmatrix} \varepsilon_m & 0 \\ 0 & \varepsilon_m + u' + \dfrac{1}{2}\left(w'\right)^2 \end{bmatrix} \tag{S.9}$$

where $\bar{g}^{\rho\beta}$ is the inverse of the metric tensor in the undeformed film, i.e., $\bar{g}^{\alpha\rho}\bar{g}_{\rho\beta}=\delta^{\alpha}_{\beta}$. The curvature tensors in the deformed and undeformed film are

$$\kappa_{\alpha\beta}=\begin{bmatrix}-\theta_{,s}w'\left(1-\xi\theta_{,s}\right) & 0\\ 0 & w''\end{bmatrix} \quad \text{and} \quad \bar{\kappa}_{\alpha\beta}=0 \tag{S.10}$$

Therefore, the curvature change tensor is

$$\Delta\kappa_{\alpha\beta}=\kappa_{\alpha\beta}-\bar{\kappa}_{\alpha\beta}=\begin{bmatrix}-\theta_{,s}w'\left(1-\xi\theta_{,s}\right) & 0\\ 0 & w''\end{bmatrix} \tag{S.11}$$

So the Lagrange strain tensor is defined as

$$E_{\alpha\beta}=\gamma_{\alpha\beta}+x_3\Delta\kappa_{\alpha\beta} \tag{S.12}$$

with two nonzero components as

$$\begin{aligned}E_{11}&=\varepsilon_m\left(1-\xi\theta_{,s}\right)^2-x_3\theta_{,s}w'\left(1-\xi\theta_{,s}\right)\\ E_{22}&=\varepsilon_m+u'+\frac{1}{2}\left(w'\right)^2+x_3w''\end{aligned} \tag{S.13}$$

where x_3 is the distance from the mid-plane of the film. The tensor the elastic constants can be defined as

$$D^{\alpha\beta\rho\mu}=\frac{E}{2(1-\nu^2)}\left[\left(\bar{g}^{\alpha\rho}\bar{g}^{\beta\mu}+\bar{g}^{\alpha\mu}\bar{g}^{\beta\rho}\right)\left(1-\nu\right)+2\upsilon\bar{g}^{\alpha\beta}\bar{g}^{\rho\mu}\right] \tag{S.14}$$

where E and ν are the Young's modulus and Poisson's ratio, respectively. The three nonzero components of $D^{\alpha\beta\rho\mu}$ are

$$\begin{aligned}D^{1111}&=\frac{E\left(\bar{g}^{11}\right)^2}{1-\nu^2}=\frac{E}{1-\nu^2}\frac{1}{\left(1-\xi\theta_{,s}\right)^4}\\ D^{2222}&=\frac{E\left(\bar{g}^{22}\right)^2}{1-\nu^2}=\frac{E}{1-\nu^2}\\ D^{1122}&=\frac{\nu E\bar{g}^{11}\bar{g}^{22}}{1-\nu^2}=\frac{\nu E}{1-\nu^2}\frac{1}{\left(1-\xi\theta_{,s}\right)^2}\end{aligned} \tag{S.15}$$

The stress-resultant tensor and the internal moment tensor are

$$T^{\alpha\beta} = hD^{\alpha\beta\rho\mu}\gamma_{\rho\mu}$$
$$M^{\alpha\beta} = \frac{h^3}{12}D^{\alpha\beta\rho\mu}\Delta\kappa_{\rho\mu} \tag{S.16}$$

Therefore, the elastic strain energy density per unit area is

$$\begin{aligned}\phi &= \frac{h}{2}D^{\alpha\beta\rho\mu}\gamma_{\alpha\beta}\gamma_{\rho\mu} + \frac{h^3}{24}D^{\alpha\beta\rho\mu}\Delta\kappa_{\alpha\beta}\Delta\kappa_{\rho\mu} \\ &= \frac{h}{2}\frac{E}{1-\nu^2}\left\{\varepsilon_m^2 + \left[\varepsilon_m + u' + \frac{1}{2}\left(w'\right)^2\right]^2 + 2\nu\varepsilon_m\left[\varepsilon_m + u' + \frac{1}{2}\left(w'\right)^2\right]\right\} \\ &+ \frac{h^3}{24}\frac{E}{1-\nu^2}\left[\frac{\left(\theta_{,s}w'\right)^2}{\left(1-\xi\theta_{,s}\right)^2} + \left(w''\right)^2 - \frac{2\nu\theta_{,s}w'w''}{1-\xi\theta_{,s}}\right]\end{aligned} \tag{S.17}$$

The stain energy of the telephone cord buckles within a period is

$$\Phi = \int_0^{s_0}\int_{-b}^{b}\phi\sqrt{g}\,d\xi ds \tag{S.18}$$

where g is the determinant of the metric tensor $g_{\alpha\beta}$ and therefore $\sqrt{g}d\xi ds$ is the element of the area. If we only keep the leading order term of $u' + \frac{1}{2}\left(w'\right)^2$, the element of area $\sqrt{g} \approx 1-\xi\theta_{,s}$. The arc-length of the centerline $s\left(x\right)$ is given by $ds = \sqrt{1+A^2q^2\cos^2\left(qx\right)}dx$. We also assume that $s=0$ at $x=0$ and $s=s_0$ at $x=2\pi/q$. From the principle of minimum potential energy, we can obtain the equilibrium equations. From $\delta\Phi/\delta u = 0$, we have

$$t_a{}' = 0 \tag{S.19}$$

where $t_a = \bar{E}_f h\sqrt{g}\left[\left(1+\nu\right)\varepsilon_m + u' + \frac{1}{2}\left(w'\right)^2\right]$ is the in-plane normal force in the film. $\bar{E}_f = \frac{E}{1-\nu^2}$ is plane strain modulus. Eq. (S.19) indicates the in-plane normal force t_a should be a constant. Similarly, from $\delta\Phi/\delta w = 0$ we obtain another differential equation

$$\left[\left(1-\xi\theta_{,s}\right)w''\right]'' - \left[\lambda w' + \frac{\theta_{,s}{}^2}{1-\xi\theta_{,s}}w'\right]' = 0 \tag{S.20}$$

where $\lambda = \dfrac{12t_a}{\bar{E}_f h^3}$. Apparently, this is an eigenvalue problem. Here, we seek a perturbative solution to Eq. (S.20) of the form

$$\begin{aligned} \lambda_n &= \lambda_n^{(0)} + \theta_{,s}\lambda_n^{(1)} + \cdots \\ w_n &= w_n^{(0)} + \theta_{,s} w_n^{(1)} + \cdots \end{aligned} \tag{S.21}$$

where λ_n and w_n are the n-th eigenvalue and eigenfunction of Eq. (S.20). Substituting Eq. (S.21) into Eq. (S.20) and comparing the power of $\theta_{,s}$ gives the following sequence of equations:

$$\frac{\partial^4 w_n^{(0)}}{\partial \xi^4} - \lambda_n^{(0)} \frac{\partial^2 w_n^{(0)}}{\partial \xi^2} = 0 \tag{S.22}$$

$$\frac{\partial^4 w_n^{(1)}}{\partial \xi^4} - \lambda_n^{(0)} \frac{\partial^2 w_n^{(1)}}{\partial \xi^2} = \frac{\partial^2}{\partial \xi^2}\left(\xi \frac{\partial^2 w_n^{(0)}}{\partial \xi^2} \right) - \lambda_n^{(1)} \frac{\partial^2 w_n^{(0)}}{\partial \xi^2} \tag{S.23}$$

with boundary conditions

$$w_n^{(i)} = 0 \quad \text{and} \quad \frac{\partial w_n^{(i)}}{\partial \xi} = 0 \quad \text{at} \quad \xi = \pm b \tag{S.24}$$

Eq. (S.22) is the zeroth order approximation of the problem. In this case, the centerline is a straight line ($\theta_{,s} = 0$). The eigenvlaue and eigenfunciton of Eq. (S.22) are

$$\lambda_n^{(0)} = -\left(\frac{n\pi}{b} \right)^2 \tag{S.25}$$

$$w_n^{(0)} = \frac{1}{\sqrt{3b}} \left[(-1)^{n+1} + \cos\left(\frac{n\pi}{b} \xi \right) \right] \tag{S.26}$$

$w_n^{(0)}$ form an orthonormal basis, i.e.,

$$\int_{-b}^{b} w_m^{(0)} w_n^{(0)} d\xi = \begin{cases} 1 & (m = n) \\ 0 & (m \neq n) \end{cases} \tag{S.27}$$

By multiplying Eq. (S.23) by $w_m^{(0)}$ and integrating it from $-b$ to b, one can find

$$\lambda_n^{(1)} = -\frac{\int_{-b}^{b} w_n^{(0)} \frac{\partial^2}{\partial \xi^2}\left(\xi \frac{\partial^2 w_n^{(0)}}{\partial \xi^2}\right) d\xi}{\int_{-b}^{b} w_n^{(0)} \frac{\partial^2 w_n^{(0)}}{\partial \xi^2} d\xi} = 0 \tag{S.28}$$

when $m = n$. By substituting $\lambda_n^{(1)} = 0$ into Eq. (S.23) and solving the equation directly, one can get

$$w_n^{(1)} = \frac{1}{4\sqrt{3b}}\left\{\xi\left[(-1)^n - \cos\left(\frac{n\pi}{b}\xi\right)\right] + \frac{n\pi}{b}\left(b^2 - \xi^2\right)\sin\left(\frac{n\pi}{b}\xi\right)\right\} + C_0 w_n^{(0)} \tag{S.29}$$

where C_0 is an unknown constant. By multiplying Eq. (S.23) by $w_m^{(0)}$ ($m \neq n$) and integrating it from $-b$ to b, one can find

$$\left(\lambda_n^{(0)} - \lambda_m^{(0)}\right)\int_{-b}^{b} w_n^{(1)} \frac{\partial^2 w_m^{(0)}}{\partial \xi^2} d\xi = 0 \tag{S.30}$$

Notice that $\lambda_n^{(0)} \neq \lambda_m^{(0)}$ when $m \neq n$. Therefore, we get $\int_{-b}^{b} w_n^{(1)} \frac{\partial^2 w_m^{(0)}}{\partial \xi^2} d\xi = 0$, which indicates $C_0 = 0$. Therefore, when $n = 1$, we get an approximation of the deflection of the plate as

$$w(x,\xi) \approx w_0\left\{\frac{1}{2}\left(1 - \frac{1}{4}\theta_{,s}\xi\right)\left[1 + \cos\left(\frac{\pi}{b}\xi\right)\right] + \frac{\pi}{4b}\theta_{,s}\left(b^2 - \xi^2\right)\sin\left(\frac{\pi}{b}\xi\right)\right\} \tag{S.31}$$

where w_0 is an unknown constant. Eq. (S.31) is reduced to $w(x,\xi) \approx \frac{1}{2} w_0\left[1 + \cos\left(\frac{\pi}{b}\xi\right)\right]$ for the buckling of a straight strip with uniform width ($\theta_{,s} = 0$). Therefore, w_0 represents the maximum deflection of the plate when $\theta_{,s} = 0$.

Notice that $t_a = \bar{E}_f h\sqrt{g}\left[(1+\nu)\varepsilon_m + u' + \frac{1}{2}(w')^2\right] = \frac{\bar{E}_f h^3 \lambda_1}{12} = -\frac{\bar{E}_f h^3}{12}\left(\frac{\pi}{b}\right)^2$. Integrate this equation from $-b$ to b, and notice that $u = 0$ at $\xi = \pm b$, one can get

$$w_0^2 = -\frac{640\left[12b^2\varepsilon_m\left(1+\nu\right)+h^2\pi^2\right]}{480\pi^2+\left(-465-110\pi^2+16\pi^4\right)b^2\theta_{,s}^2} \tag{S.32}$$

Eq.(S.31) together with Eq.(S.32) provides an analytical solution to the 3D profile of the TC buckle after its projected area is available.

Supplementary Note 2: Measurable A'/λ and λ/b in various TC blisters shown in Supplementary Figure 2

We have measured the values of A'/λ and λ/b in various TC blisters according to the optical or AFM images reported in the literatures [1-27]. The values of A'/λ and λ/b for each kind of materials are estimated as the average by several measurements.

Supplementary Note 3: Method to simulate evolution of the telephone cord buckle

Supplementary Figure 3 shows the side undulation curve under different values of A/λ at b/h=49, $\lambda/b=2$ to set the pre-delamination area in our numerical simulation.

We perform the numerical simulation for the effect of A/λ on the post-buckling morphology of the compressed plate on the substrate given the parameters $\varepsilon_{\alpha\beta}^0=\varepsilon_m\delta_{\alpha\beta}$, $\varepsilon_m=0.005$ $\mu_f/\mu_s=2.5$, $\nu_f=0.3$, $\nu_s=0.5$, $\Gamma_{\Lambda_i}^*=\Gamma_{\Lambda_i}/\Gamma_\zeta=0.01$, b/h=49, $\lambda/b=2$, as shown in Supplementary Figure 4. The simulated result in Figure 3 about the dependence of b_1/b_2 and $w_{C-line}^{\max}/w_{B-line}^{\max}$ on A/λ is extracted from the data in Supplementary Figure 4.

Supplementary Figure 5 shows the effect of modulus ratio between film and

substrate on the post-buckling morphology of the compressed plate on the substrate given the parameters $\varepsilon_m = 0.005, v_f = 0.3,\ v_s = 0.5,$, *b/h*=49, $\lambda / b = 2,$ *A*/λ=0.08. It is found that the larger modulus ratio leads to larger energy releasing rate and maximum deflection of the TC blister. Interestingly, the asymmetry characterized by $w_{C-line}^{\max} / w_{B-line}^{\max}$ becomes weak as the substrate is compliant, i.e. $\mu_f / \mu_s = 20$. This may indicate that it does not always happens. More detailed study is needed in future.

The simulated result in Supplementary Figure 6 is obtained by numerically solving the above outlined continuum model in a computational cell with periodic boundary conditions using input parameters: the cell size 2048h×2048h with an initial circular delamination nuclei of radius *r*=5*h* , $\varepsilon_{\alpha\beta}^0 = \varepsilon_m \delta_{\alpha\beta}, \varepsilon_m = 0.022$ $\mu_f / \mu_s = 5,$ $v_f = 0.3$, $v_s = 0.5$, $\Gamma_{\Lambda_i}^* = \Gamma_{\Lambda_i} / \Gamma_\zeta = 0.01$, $\delta_n = 0.2h$, $\delta_t = \delta_n$, $\gamma_n^* = \gamma_n / e\delta_n\mu_s = 0.02$ and $\gamma_t^* = \gamma_t / e\delta_n\mu_s = 0.1$.

Supplementary References

[1] S. J. Yu, Y. J. Zhang, and M. G. Chen, Thin Solid Films **518**, 222 (2009).

[2] M. He, C. Gaire, G.C. Wang, and T.M. Lu, Micro. Reliab. **51**, 847 (2011).

[3] Q. L. Ye, and S. J. Yu, Philos. Mag. Lett. **93**, 710 (2013).

[4] K. Xiao, Z. S. Guan, G. J. Wang, L. Jiang, D. B. Zhu, and Y. R. Wang, Appl. Phys. Lett. **85**, 1934 (2004).

[5] N. R. Moody, D. P. Adams, M. J. Cordill, D. F. Bahr, and A. A. Volinsky, Symposium on Thin Films, SAND2003-8146C (2003).

[6] A. Lee, C. S. Litteken, R. H. Dauskardt, and W.D. Nix, Acta Materialia **53**, 609 (2005).

[7] M. J. Cordill, N. R. Moody, and D. F. Bahr, Acta Mater. **53**, 2555 (2005).

[8] P. Waters, and A. A. Volinsky, Exper. Mech. **47**, 163 (2007).

[9] A. A. Taylor, M. J. Cordill, L. Bowles, J. Schalko, and G. Dehm, Thin Solid Films **531**, 354 (2013).

[10] P. Goudeau, P. O. Renaul, P. Villain, C. Coupeau, V. Pelosin, B. Boubeker, K. F. Badawi, D. Thiaudi ère, and M. Gailhanou, Thin Solid Films **398**, 496 (2001).

[11] J. Y. Faou, G. Parry, S. Grachev, and E. Barthel, Phys. Rev. Lett. **108**, 116102 (2012).

[12] H. Y. Yu, C. kim, and S. C. Sanday, Thin Solid Films **196**, 229 (1991).

[13] A. A Volinsky, Mat. Res. Soc. Symp. Proc. **749**, W10.7.1 (2003).

[14] A. A.Volinsky, J. B. Vella, and W. W.Gerberich, Thin Solid Films **429**, 201 (2003).

[15] Z. J. Liu, N. Jiang, Y. G. Shen, and X. Li, Thin Solid Films **516**, 7609 (2008).

[16] J. P. McDonald, V. R. Mistry, K. E. Ray, and S. M. Yalisove, Appl. Phys. Lett. **88**, 183113 (2006).

[17] J. Y Faou, G. Parry, S. Grachev, and E. Barthel, J. Mech. Phys. Solids **75**, 93 (2015).

[18] S. Y. Grache, A. Mehlich, J. D. Kamminga, E. Barthel, and E. S ønderg ård, Thin Solid Films **518**, 6052 (2010) 4.

[19] G. Gilles, and B. Rau, Thin Solid Films **120**, 109 (1984).

[20] S. B. Iyer, K. S. Harshavardhan, and V. Kumar, Thin Solid Films **256**, 94 (1995).

[21] M. W. Moon, H. M. Jensen, J. W. Hutchinson, K. H. Oh, and A. G. Evans, J. Mech. Phys. Solids **50**, 2355 (2002).

[22] D. He, W. Cheng, J. Qin, J. Yue, E. Xie, and G. Chen, Appl. Surf. Sci. **191**, 338 (2002).

[23] X. D. Zhu, K. Narumi, and H. Naramoto, J. Phys.: Condens. Matter **19**, 236227 (2007).

[24] S. Peponas, M. Lejeune, S. Charvet, M. Guedda, and M. Benlahsen, Surf. Coat. Technol. **212**, 229 (2012).

[25] M. D. Thouless, J. Am. Ceram. Soc. **76**, 2936 (1993).

[26] S. J. Yu, M. G. Chen, J. Chen, H. Zhou, Y. J. Zhang, and P. Z. Si, Surf. Coat. Technol. **228**, 258 (2013).

[27] S. J. Yu, Y. C. Shi, M. G. Chen, P. Z. Si, Y. Zhou, X. F. Zhang, J. Chen, H. Zhou, and Z. W. Jiao, Surf. Coat. Technol. **232**, 884 (2013).

[28] Y. Ni and A.K. Soh, Acta Mater. **69**, 37 (2014).